

Radiation damage haloes in biotite investigated using high-resolution transmission electron microscopy[‡]

WILLIAM R. BOWER^{1,2,*}, RICHARD A.D. PATTRICK^{1,2}, CAROLYN I. PEARCE³, GILES T.R. DROOP¹,
AND SARAH J. HAIGH⁴

¹School of Earth, Atmospheric and Environmental Sciences, University of Manchester, Manchester, M13 9PL, U.K.

²Research Centre for Radwaste Disposal, University of Manchester, Manchester, M13 9PL, U.K.

³School of Chemistry & Dalton Nuclear Institute, University of Manchester, Manchester, M13 9PL, U.K.

⁴School of Materials, University of Manchester, Manchester, M13 9PL, U.K.

ABSTRACT

The complex, nanometer-scale structural changes resulting from long-term α -particle bombardment of the mineral biotite are revealed for the first time using high-resolution transmission electron microscope (HRTEM) imaging. Radiohaloes are the product of high-energy α -particles emitted from radioactive inclusions penetrating into the surrounding mineral over long (~1.8 Ga) timescales, resulting in intense discoloration attributed to ionization events and structural damage. HRTEM analysis of these radiohaloes reveals the long-term breakdown of the biotite structure into three distinct domains. Nanometer-scale, neo-phase regions of dilated and contracted mica structure, with periodicities comparable to 1:1 phyllosilicates, are bound by semi-amorphous, high-defect density domains. These are periodically interspersed with areas of near-original biotite structure. Across the halo region, damaged crystallites have become misoriented, revealing changes in the mica layer-to-layer spacing. This nanoscale response of the mica structure has profound implications for understanding the performance of phyllosilicates in barrier systems employed in the safe isolation of nuclear waste, as materials such as these will be relied upon to retard radionuclide migration over the lifetime of a geological disposal facility.

Keywords: Radiation damage, radiohaloes, phyllosilicates, mica, biotite, high-resolution transmission electron microscopy, geological disposal

INTRODUCTION

Deep-geologic isolation is currently the favored solution for addressing the global problem of long-term radioactive waste storage, and phyllosilicates, such as mica and clays, will be key components within all geological disposal facilities (GDF). These materials act as inorganic ion exchangers and are highly reactive; thus their presence in a GDF will be an essential barrier to radionuclide mobility (NDA 2010; DECC 2014). Both in the near field, as potential “sinks” for radionuclides following canister failure (clay backfill material) and in the far-field as a result of radionuclide migration via fluid ingress (phyllosilicates in the host rock), phyllosilicates will be subjected to radiation damage levels that may alter their efficiency as barrier materials. Structural changes resulting from long term α - and γ -irradiation can have a major effect on the sorption capacity and reactivity of these sheet silicates and a detailed understanding of this is crucial to predict the safe performance of a GDF over timescales of up to 10^6 years. In addition, the study of radiation damage mechanisms in minerals and ceramics is applicable to nuclear waste form durability (Ewing 1999, 2001; Ewing et al. 2000, 2003).

Radiohaloes in biotite

Radiation damage haloes in phyllosilicates are a widespread phenomenon and spherical “radiohaloes” surrounding 1.8 billion year old monazite inclusions (U and Th rich) in biotite provide a unique opportunity for long-term radiation stability assessments in natural minerals (Nasdala et al. 2001, 2006; Pal 2004; Patrick et al. 2013). Biotite mica is a sheet silicate defined by repeated tetrahedral-octahedral-tetrahedral (TOT) layers in which sheets of metal-rich octahedra are “sandwiched” between sheets of silica tetrahedra arranged in hexagonal rings. OH⁻ groups occupy the voids between the rings of tetrahedra and potassium interlayer cations separate and bind the TOT layers (Fleet et al. 2003; Brigatti et al. 2008). Consequently, the large interlayer region (ca. 3.5 Å) can accommodate α -emitting radionuclides such as uranium (Ames et al. 1983; Hudson et al. 1999), as well as other harmful radionuclides with lower sorption potentials such as cesium-137; this property is of major significance for radionuclide isolation (Komarneni and Roy 1988; Fuller et al. 2015). The distance between neighboring octahedral sheets is typically consistent at ca. 1 nm.

Radiohaloes in biotite and other phyllosilicates are manifested as spheres of discoloration, approximately 70 μ m in diameter, surrounding radioactive inclusions that contain α -emitters such as U²³⁸ and Th²³². Such haloes result from α -particles (⁴He²⁺

* E-mail: william.bower@manchester.ac.uk

[‡] Open access: Article available to all readers online.

ions) penetrating beyond the host inclusion and creating defects in the surrounding mineral as they lose energy through ionization and atomic collisions. Alpha-particles in the U^{238} and Th^{232} decay chains leave their source with an initial energy of 4–8 MeV, depending on the parent isotope. Thereafter, the density, chemistry, and structure of the surrounding phase determines the rate of energy loss and dictates the radius at which the positively charged ions lose sufficient energy to permit nuclear interactions, causing on the order of hundreds of atomic displacements. Alpha-particles (at the energies in this range) have both inelastic (electronic) and elastic (nuclear) contributions to their stopping power in solid media. This is in contrast to proton beams, for example, which have a negligible elastic contribution due to their lower mass. The electronic contribution to an α -particle's stopping power is initially dominant; an α 's ionization potential increases to a "Bragg Peak" with respect to penetration distance. Following sufficient energy loss to ionization events, an α -particle's nuclear interaction cross section increases, with the peak of structural damage (knock-on displacements) occurring in a narrow band at the end of the particle's range (see Fig. 1). By the end of its trajectory the α -particle has captured electrons and can therefore be considered a neutral helium atom (Lieser 1997).

Under this model of energy loss, it is predicted that the highest level of structural damage across a radiohalo will be over the final few micrometers of an α -particle's trajectory, however differing densities and morphologies of inclusions may lead to a heterogeneous accumulation of structural damage across a halo region. Where α dose is constrained by time or limited U/Th concentrations in the inclusion, discrete, dark spheres develop (seen as rings in cross section) at a specific radius from the point source, corresponding to the penetration distance of the

α -particles at different energies (Demayo et al. 1981; Pal 2004). Such dark rings correspond to the theorized maximum region of structural damage for an α -particle of a discrete energy; it has therefore been reported that point defects contribute primarily to color change (Nasdala et al. 2001). After prolonged exposure, areas of extensive radiation damage become more pervasive and the rings are lost, yielding a single, optically dark sphere of damage (Fig. 2a). Where the diameter of the inclusion is large (i.e., a substantial proportion of the α -particle's penetration range), discoloration has been shown to match the morphology of the emitter, rather than forming perfect spheres, as there is a higher probability that an α -particle will dissipate its energy within the host lattice (Bower et al. 2016).

EXPERIMENTAL METHODS

Sample characterization

The biotite in this study is taken from a 1.8 Ga almandine-biotite-grunerite rock from Tunaberg, Sweden; containing abundant, micrometer-scale inclusions of Th-rich monazite ($Ce_{0.40}La_{0.22}Nd_{0.12}Pr_{0.04}Sm_{0.05}Th_{0.15}U_{0.02}Si_{0.02}PO_4$) (Patrick et al. 2013); this is the primary α -emitter in the sample. In the thin sections examined, apart from within the radiohaloes, there was no evidence of alteration of the biotite. In a prior study into these radiohaloes undertaken by Patrick et al. (2013) the average α -particle fluence across the haloes was quoted as 0.022 α per atomic component of the monazite inclusions ($r = ca. 30 \mu m$). In the same study, synchrotron-based, microfocus X-ray diffraction and X-ray absorption spectroscopy analysis demonstrated short-range structural disruption across these radiohaloes and this was postulated to represent the development of new structural domains.

Electronprobe microanalysis (EPMA) on the biotite, used to determine the structural formulas 1 and 2 showed very little change in chemistry across the haloes on a micrometer scale, however changes such as K^+ inhomogeneities over nano-scale regions (see results and discussion) would not be revealed through this method due to the scale of analysis ($\sim 1 \mu m$).

Outside halo: $(Na_{0.02}K_{0.97})(Mg_{0.94}Fe_{1.94}Al_{0.18}Ti_{0.02}Mn_{0.047})[Si_{2.947}Al_{1.13}O_{10}/(OH)_2]$ (1)

Inside halo: $(Na_{0.02}K_{0.97})(Mg_{0.91}Fe_{1.94}Al_{0.17}Ti_{0.02}Mn_{0.046})[Si_{2.938}Al_{1.15}O_{10}/(OH)_2]$ (2)

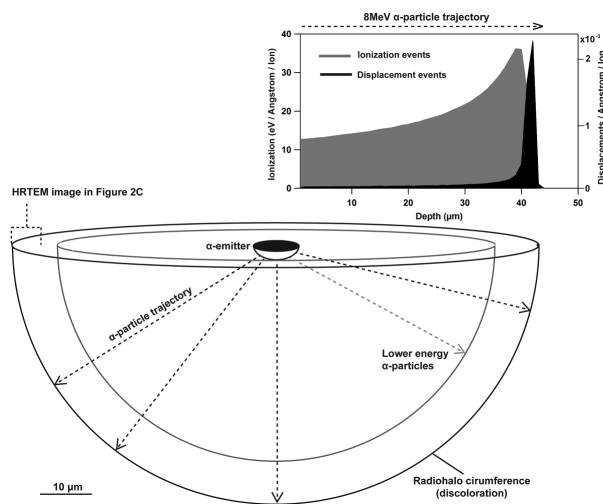


FIGURE 1. Cross-sectional schematic of a radiohalo (adapted from Gentry 1992), with inset graph displaying the energy loss of an 8 MeV α -particle into a model biotite density/chemistry. The ionization/nuclear interaction curves were modeled using the software Stopping and Range of Ions in Matter (SRIM) (Ziegler 2013). Theoretically, the region of maximum structural damage occurs at the outer edge of the halo (the end of the particle's range). The approximate region for the HRTEM image in Figure 2c is marked.

Sample preparation

HRTEM imaging is the ideal technique to explore radiation damage mechanisms and for studying the distribution of resulting defect structures (Veblen et al. 1993). To isolate the radiohaloes for analysis by HRTEM, areas of abundant radiohaloes in biotite were identified in a $30 \mu m$ optically "thin" mineral section and marked; the section was then floated from its glass substrate and carefully mounted onto a 3 mm diameter copper slot grid, positioning the radiohalo across the center of the grid slot. The copper grid provides support during further thinning. An Ar^+ sputtering Precision Ion Polishing System (PIPS) with a custom built stage was used to obtain a specimen thickness suitable for HRTEM imaging across the radiohalo. Optical image overlays were used to locate the thinnest areas of the biotite specimen containing the radiohaloes as the optical contrast of the halo is greatly reduced for the thinned samples.

High-resolution transmission electron microscopy

The $40 \mu m$ diameter haloes were analyzed and high-resolution images collected using an FEI Titan ChemiSTEM G2 80-200 S/TEM in the University of Manchester's School of Materials. The microscope was operated in high-resolution TEM imaging mode with an accelerating voltage of 200 kV. Electron diffraction patterns were obtained from the same instrument using a $40 \mu m$ selected area aperture. Fast Fourier transforms of selected regions within an individual HRTEM image were made using the Gatan DigitalMicrograph software (ver. 2.31.734.0).

RESULTS

The HRTEM image presented in this study was taken from within the damage halo (ca. 25–30 μm from the α -emitter) and is compared with the biotite ca. 250 μm outside the discolored halo region, within the same single crystal (Fig. 2). The latter, undamaged crystal viewed along [131] is shown in Figure 2b;

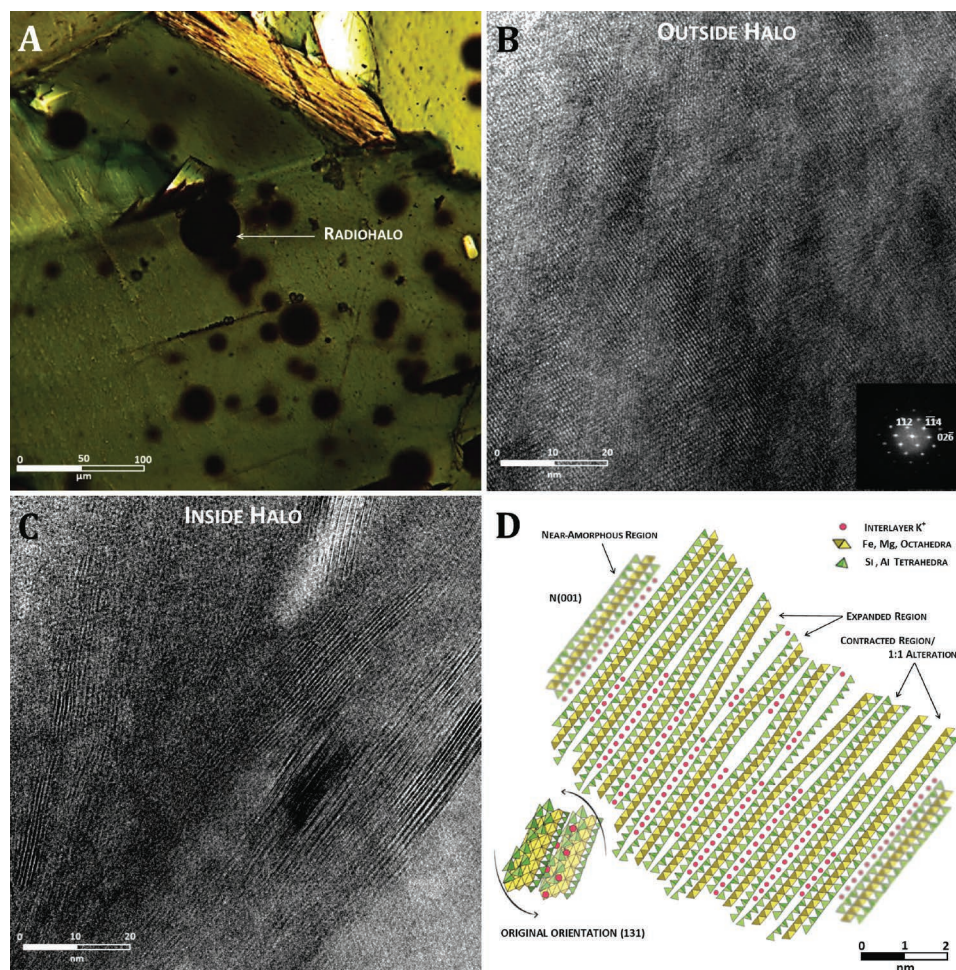
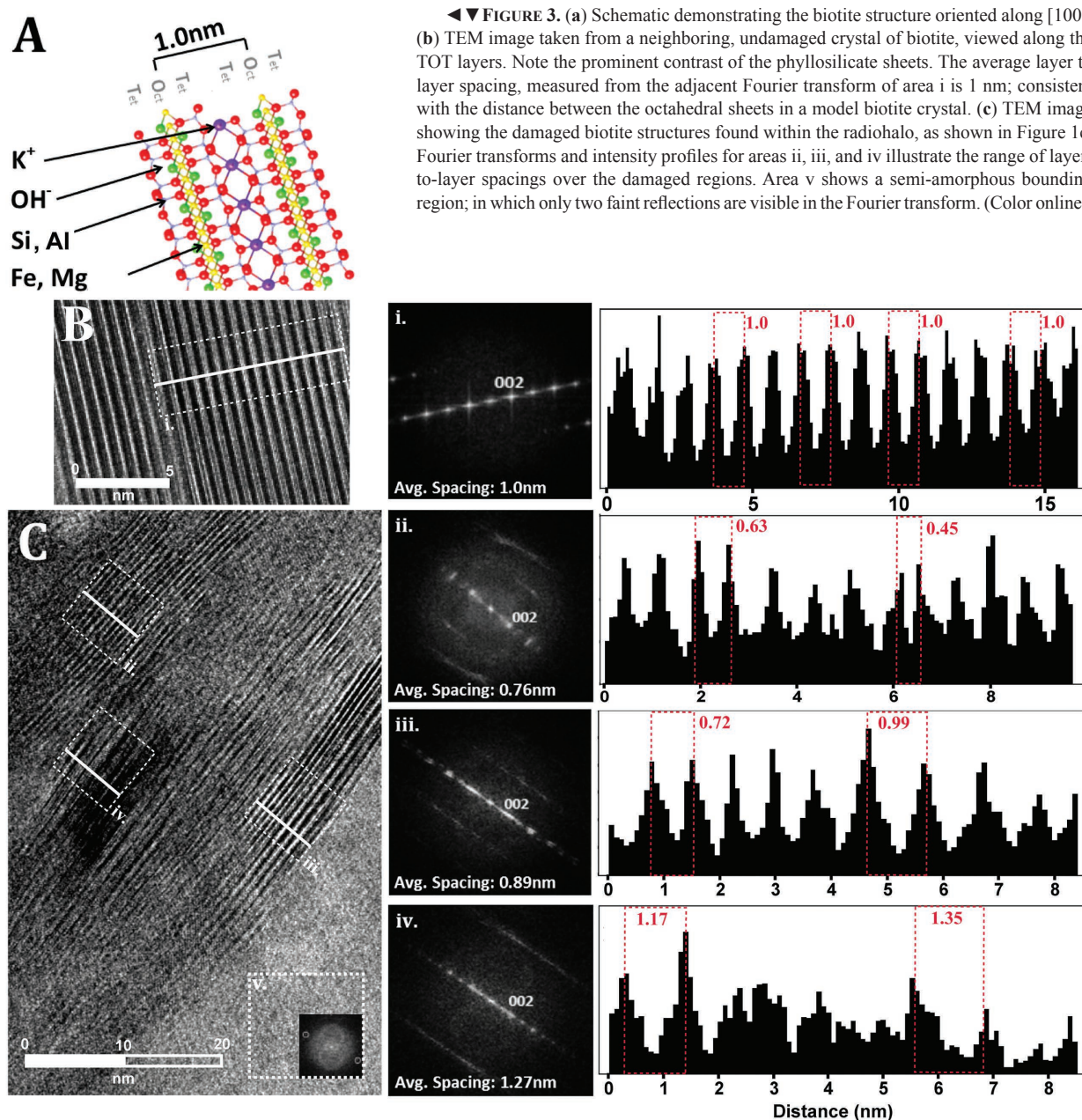


FIGURE 2. (a) Optical microscope image of abundant, intensely darkened radiohaloes surrounding monazite (Th-rich) inclusions within biotite crystals. Discolored haloes result from radiation damage caused by α -particle bombardment over geologic timescales. Note that the differences in sizes of the haloes in this image stem from the different depths at which the haloes have been cross-sectioned. (b) HRTEM image of an area of unirradiated biotite crystal, outside of the halo area. Inset Fourier transform of this image demonstrates the periodicity of the biotite, oriented along [131]. (c) HRTEM image of an area of biotite inside the dark radiohalo, showing significant structural disturbance as a result of α -particle irradiation. Note the varied orientation of several discrete nanoscale regions including near-amorphous areas. (d) Schematic representation of the damaged crystal shown in c. Near-amorphous regions enclose neo-domains of radiation-damaged structure, displaying expansion and contraction of the silicate layers over nanometer-scale regions. Interlayer K^+ has likely been liberated or relocated across the crystal. Note the misorientation of the domains from the undamaged structure orientation [131] to the damaged regions that are close to $[hk0]$.

with the inset Fourier transform highlighting the uninterrupted periodic structure beyond the radiohalo. In complete contrast, the HRTEM image from within the α -particle damage halo shows extensive distortion, with major disturbances in the long-range periodicity discernible over the whole area (Fig. 2c). Three distinct structural domains are present in the zones of structural damage: (1) regions of the original, crystalline biotite structure, retained in the same [131] orientation as the “perfect” crystal outside the halo; (2) near-amorphous regions (traces of periodicity defined by minor “reflections” in reciprocal space); and (3) nanometer-sized neo-phase domains that are rotated compared to the host crystal. When viewed along the TOT layers these latter regions displayed non-uniform, basal plane expansion

and contraction; highlighted by the boxed regions, see Fourier transform analysis and the series of contrast profiles in Figure 3. The near-amorphous regions are areas of biotite that have suffered near-complete loss of periodicity are shown by inset (v) in Figure 3c. These can be interpreted as the result of direct atomic displacement by α -particles, resulting in regions of dense Frenkel defect accumulation (shown as area v in Fig. 3c). The images display a non-uniform distribution of these near-amorphous regions with respect to the α -emitter; while conventional energy deposition models show a time averaged distribution of damage over an α -particle’s track, at this scale the stochastic effect of radiation damage is apparent and the spatial evolution of these high defect regions is poorly constrained. Local variations in α -particle col-



◀▼ **FIGURE 3.** (a) Schematic demonstrating the biotite structure oriented along [100]. (b) TEM image taken from a neighboring, undamaged crystal of biotite, viewed along the TOT layers. Note the prominent contrast of the phyllosilicate sheets. The average layer to layer spacing, measured from the adjacent Fourier transform of area i is 1 nm; consistent with the distance between the octahedral sheets in a model biotite crystal. (c) TEM image showing the damaged biotite structures found within the radiohalo, as shown in Figure 1c. Fourier transforms and intensity profiles for areas ii, iii, and iv illustrate the range of layer-to-layer spacings over the damaged regions. Area v shows a semi-amorphous bounding region; in which only two faint reflections are visible in the Fourier transform. (Color online.)

lisions can lead to regions of relatively high defect density that can subsequently act as zones of nucleation for further damage/eventual amorphization and explain the heterogeneous spatial distribution of the damage accumulation. Such near-amorphous regions surround the neo-phase domains (areas ii to iv in Figure 3), it is likely that these represent areas of weakness along which the pseudo-structural domains have rotated.

DISCUSSION

Structural changes will radically alter the mineral's interactions with radionuclide species in solution. Layer distortions and amorphous regions could promote radionuclide uptake and incorporation, whereas changes to the layer-to-layer spacing could potentially reduce the mineral's cation exchange capacity.

The schematic in Figure 2d displays along-layer heterogeneity and demonstrates the possibility for interlayer K^+ loss, likely leaving the bare tetrahedral sheets in need of charge balancing.

As shown in Figure 3, the layer-to-layer spacings within the discrete, neo-formed domains are highly variable. Certain regions (area ii in Fig. 3c) display reduced layer-to-layer spacings (0.76 nm) in comparison to a reference region of the undamaged biotite in a neighboring crystal. The interlayer spacing of area ii in Figure 3c is consistent with the layer-to-layer spacing of kaolinite (Ahn and Peacor 1987), a common 1:1 weathering product of micas. Other regions (area iv) show a less consistent expansion of the layers, with an average spacing of 1.27 nm, more comparable with that of vermiculite (Veblen 1985). Highly localized variations in layer-to-layer spacing have previously been observed in

TEM investigations of biotite transformations (Ahn and Peacor 1987; Murakami et al. 2003; Cruz and Nieto 2006). In weathered biotite, regions as small as 5 nm^3 contain layer-to-layer spacings of 0.7 nm that were attributed to the development of the 1:1 phyllosilicate kaolinite along permeable zones. In addition, biotite-vermiculite interlayers and domains of vermiculite were observed in an experimental study of the breakdown of biotite; vermiculite has layer-to-layer spacings of up to 1.515 nm (depending on hydration state) (Veblen 1985; Reichenbach et al. 1995). The layer-by-layer breakdown of biotite to vermiculite and/or kaolinite involves loss of interlayer K (Murakami et al. 2003) (although the process is generally retarded in high Fe biotite, such as the sample in this study).

The observed neo-formed regions, bound by near-amorphous areas (Fig. 3), are interpreted as extremely localized biotite breakdown to neo-formed phyllosilicates, by the loss of interlayer cations and OH-groups (see Patrick et al. 2013). The high density of point and extended defects will have facilitated localized transport of the released components and may have aided recrystallization. The absence of such defects elsewhere outside the radiohalo is evidence that α -particle damage may enhance biotite breakdown over long timescales, even at relatively low particle fluences, such that recrystallization can occur without an overwhelming loss of periodicity.

The abundance of the expanded and contracted regions will cause a significant overall change in strain distribution across the crystal, as well as the combined products of localized atomic displacements and the development of the broader amorphous domains. The differential crystal stresses, resulting from the structural aberrations has caused the TOT layers and their weak interlayers to twist and “concertina”; thus allowing multiple orientations to be observed across one 100 nm^2 area. The propensity for crystal expansion/contraction around a radiocenter as a product of radiation damage has been previously documented (Ewing et al. 2000; Harfouche et al. 2005). This study has identified more extensive effects of α -particle damage across radiohaloes than the detailed work by Nasdala et al. (2001); likely as a result of significantly higher fluences calculated across the radiohaloes in the sample examined here.

Precision ion polishing

An important consideration for imaging radiation damage effects is the need to isolate preparation-induced lattice damage from the areas of crystal under analysis. Thinning via the Precision Ion Polishing System (PIPS) is achieved by sputtering Ar ions across the top and bottom surfaces of the sample, which inevitably induces an amorphous layer on the top and bottom surfaces of the sample, and is most visible in the thinnest crystal edge region. Figure 4 highlights this PIPS induced damage—a narrow amorphous band lining the edge of the crystal, adjacent to a wholly crystalline region of biotite. It should also be noted that outside the radiohalo, areas of unaltered, original biotite structure are apparent, shown in Figure 2 and Figure 4c. None of the distortions observed inside the radiohalo were observable in the original crystal thus the structural changes observed are not attributable to metamorphism-induced strain/dislocations experienced by the rock formation, weathering products or specimen preparation induced artifacts. To investigate the changes induced

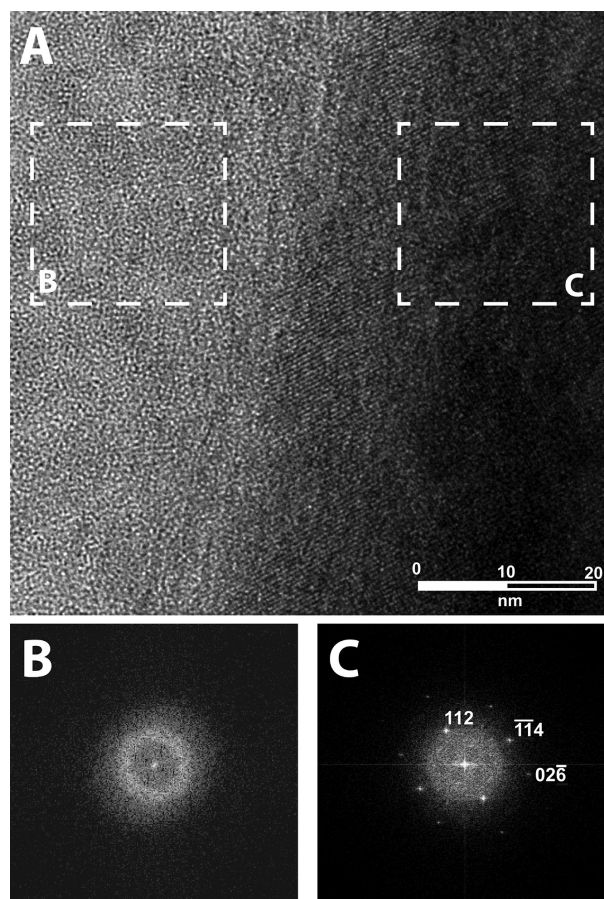


FIGURE 4. (a) HRTEM image showing PIPS induced amorphization within a crystal of biotite adjacent to a thinned edge, outside of the radiohalo region. Fourier transforms from the areas marked **b** and **c** are displayed below the HRTEM image. Note the presence of pristine biotite structure directly adjacent to the thinned area, displaying none of the structural effects observed within the radiohalo region.

by exposure to the electron beam during imaging, pristine areas of the sample were exposed to prolonged HRTEM imaging. This irradiation produced a gradual increase in amorphization and a mottled surface appearance but no structural changes similar to those seen within the radiohalo were observed.

IMPLICATIONS

The images analyzed here demonstrate nanometer-scale structural heterogeneity as a product of α -particle radiation damage, reducing a homogeneous, laterally continuous crystal into discrete domains of amorphization and distorted neo-phase domains. Thus, the interaction of radiation-damaged phases with radionuclides will be very different from the unaltered mineral structures, both in terms of their sorption capacity and reactivity. This provides an atomic-level understanding of the long-term effects of radiation damage in phyllosilicates, which is both essential for modeling radionuclide mobility and containment as well as the elucidation of the true nature of this widespread phenomenon.

This study demonstrates the potential difficulty in model-

ing the effect of radiation damage across bulk phyllosilicate phases, to predict the expected reactivity and sorption capacity of radiation-damaged and altered minerals, because of the inhomogeneity and the interconnected effects of the structural distortions seen in the HRTEM images. For example, mica dissolution is thought to occur at edge sites; thus the development of new edge sites shown here has the potential to substantially increase the reactive surface area of these minerals (Rufe and Hochella 1999). In complex systems such as these, it is clear that complete amorphization is not the only long-term consequence of prolonged irradiation, indeed several relatively stable pseudo-structures may form as intermediate, partial breakdown products. The extreme variations in structural damage and consequent mineral alteration over such small regions will be an important factor to consider when assessing the long-term performance of phyllosilicates in both the engineered and natural barriers in any nuclear waste disposal facility.

ACKNOWLEDGMENTS

W.R.B. and R.A.D.P. acknowledge the National Environment Research Council (NERC) for project funding under grant NE/K500859/1 and Diamond Light Source, Harwell, U.K., for beamtime allocated for both work cited here and for future work.

S.J.H. acknowledges funding support from the Defense Threat Reduction Agency under grant HDTRA1-12-1-0013 and the Engineering and Physical Sciences research council (EPSRC), U.K. The Titan ChemiSTEM was purchased with funding support from the HM Government (U.K.) and is associated with the capabilities of the University of Manchester's Nuclear Manufacturing Centre.

REFERENCES CITED

- Ahn, J.H., and Peacor, D.R. (1987) Kaolinitization of biotite: TEM data and implications for an alteration mechanism. *American Mineralogist*, 72, 353–356.
- Ames, L.L., McGarrah, J.E., and Walker, B.A. (1983) Sorption of uranium and radium by biotite, muscovite and phlogopite. *Clays and Clay Minerals*, 31, 343–351.
- Bower, W.R., Pearce, C.I., Droop, G.T.R., Mosselmans, J.F.W., Geraki, K., and Patrick, R.A.D. (2016) Radiation damage from long term alpha particle bombardment of silicates - a microfocus XRD and Fe K-edge XANES study. *Mineralogical Magazine*, in press.
- Brigatti, M.F., Guidotti, C.V., Malferrari, D., and Sassi, F.P. (2008) Single-crystal X-ray studies of trioctahedral micas coexisting with dioctahedral micas in metamorphic sequences from western Maine. *American Mineralogist*, 93, 396–408.
- Cruz, M.D.R., and Nieto, J.M. (2006) Chemical and structural evolution of "metamorphic vermiculite" in metaclastic rocks of the Betic Cordillera, Málaga, Spain: A synthesis. *Canadian Mineralogist*, 44, 249–265.
- DECC (2014) Implementing Geological Disposal. White Paper, Department of Energy and Climate Change. URN 14D/235.
- Demayo, B., Seal, M., and Vance, E.R. (1981) Optical spectra of giant radiohaloes in Madagascar biotite. *American Mineralogist*, 66, 358–361.
- Ewing, R.C. (1999) Nuclear waste forms for actinides. *Proceedings of the National Academy of Sciences*, 96, 3432–3439.
- (2001) The design and evaluation of nuclear-waste forms: clues from mineralogy. *Canadian Mineralogist*, 39, 697–715.
- Ewing, R.C., Meldrum, A., Wang, L., and Wang, S. (2000) Radiation-Induced Amorphization. *Reviews in Mineralogy and Geochemistry*, 39, 319–361.
- Ewing, R.C., Meldrum, A., Wang, L., Weber, W.J., and Corrales, L.R. (2003) Radiation effects in zircon. *Reviews in Mineralogy and Geochemistry*, 53, 387–425.
- Fleet, M.E., Deer, W.A., Howie, R.A., and Zussman, J. (2003) *Rock-forming Minerals: Micas*, Second., 765 p. Vol. 3A. The Geological Society, London.
- Fuller, A.J., Shaw, S., Ward, M.B., Haigh, S.J., Mosselmans, J.F.W.M., Peacock, C.L., Stackhouse, S., Dent, A.J., Trivedig, D., and Burke, I.T. (2015) Caesium incorporation and retention in illite interlayers. *Applied Clay Science*, 108, 128–134. <http://dx.doi.org/10.1016/j.clay.2015.02.008>.
- Genry, R.V. (1992) *Creation's Tiny Mystery*, 3rd edition. Earth Science Associates, Knoxville, Tennessee.
- Harfouche, M., Farges, F., Crocombette, J.P., and Flank, A.M. (2005) XAFS and molecular dynamics study of natural minerals, analogs of ceramics for nuclear waste storage. *Physica Scripta*, 2005, 928.
- Hudson, E.A., Terminello, L.J., Viani, B.E., Denecke, M., Reich, T., Allen, P.G., Bucher, J.G., Shuh, D.K., and Edelman, N.M. (1999) The structure of U⁶⁺ sorption complexes on vermiculite and hydrobiotite. *Clays and Clay Minerals*, 47, 439–497.
- Komarneni, S., and Roy, R. (1988) A cesium-selective ion sieve made by topotactic leaching of phlogopite mica. *Science*, 239, 1268–1288.
- Lieser, K.H. (1997) *Nuclear and Radiochemistry: Fundamentals and Applications*, 1st ed., 1, 472 p. Wiley, New York.
- Murakami, T., Utsunomiya, S., Yokoyama, T., and Kasama, T. (2003) Biotite dissolution processes and mechanisms in the laboratory and in nature: Early stage weathering environment and vermiculitization. *American Mineralogist*, 88, 377–386.
- Nasdala, L., Wenzel, M., Andrut, M., Wirth, R., and Blaum, P. (2001) The nature of radiohaloes in biotite: Experimental studies and modeling. *American Mineralogist*, 86, 498–512.
- Nasdala, L., Wildner, M., Wirth, R., Groschopf, N., Pal, D.C., and Möller, A. (2006) Alpha particle haloes in chlorite and cordierite. *Mineralogy and Petrology*, 86, 1–27.
- NDA (2010) *Geological Disposal: Steps Towards Implementation*. NDA Report no. NDA/RWMD/013.
- Pal, D.C. (2004) Concentric rings of radioactive halo in chlorite, Turamdih uranium deposit, Singhbhum Shear Zone, Eastern India: a possible result of ²³⁸U chain decay. *Current Science*, 87, 662–667.
- Patrick, R.A.D., Charnock, J.M., Geraki, T., Mosselmans, J.F.W., Pearce, C.I., Pimblott, S., and Droop, G.T.R. (2013) Alpha particle damage in biotite characterised by microfocus X-ray diffraction and Fe K-edge X-ray absorption spectroscopy. *Mineralogical Magazine*, 77, 2867–2882.
- Reichenbach, H., Graf, V., and Beyer, J. (1995) Dehydration and rehydration of vermiculites II: Phlogopitic Ca-vermiculite. *Clay Minerals*, 30, 273–286.
- Rufe, E., and Hochella, M.F. (1999) Quantitative assessment of reactive surface area of phlogopite during acid dissolution. *Science*, 285, 874–876.
- Veblen, D.R. (1985) Extended defects and vacancy non-stoichiometry in rock-forming minerals. *Geophysical Monograph Series*, 31, 122–131.
- Veblen, D.R., Banfield, J.F., Guthrie, G.D. Jr., Heaney, P.J., Ilton, E.S., Livi, K.J., and Smelik, E.A. (1993) High-resolution and analytical transmission electron microscopy of mineral disorders and reactions. *Science*, 260, 1465–1472.
- Ziegler, J.F. (2013) *The Stopping and Range of Ions in Matter*, Software. <http://www.srim.org/>, accessed on January 10, 2013.

MANUSCRIPT RECEIVED MARCH 10, 2015

MANUSCRIPT ACCEPTED MAY 3, 2015

MANUSCRIPT HANDLED BY LYNDA WILLIAMS